DNA Nanoflower Eye Drops with Antibiotic-Resistant Gene Regulation Ability for MRSA Keratitis Target Treatment

Ran, Meixin; Sun, Rong; Yan, Jiaqi; Pulliainen, Arto T.; Zhang, Yu; Zhang, Hongbo

Published in:
Small

DOI:
10.1002/smll.202304194

Published: 01/11/2023

Document Version
Final published version

NANO · MICRO small
www.small-journal.com

DNA Nanoflower Eye Drops with Antibiotic-Resistant Gene Regulation Ability for MRSA Keratitis Target Treatment

Meixin Ran, Rong Sun, Jiaqi Yan, Arto T. Pulliainen, Yu Zhang, and Hongbo Zhang**

Methicillin-resistant *Staphylococcus aureus* (MRSA) biofilm-associated bacterial keratitis is highly intractable, with strong resistance to β-lactam antibiotics. Inhibiting the MRSA resistance gene mecR1 to downregulate penicillin-binding protein PBP2a has been implicated in the sensitization of β-lactam antibiotics to MRSA. However, oligonucleotide gene regulators struggle to penetrate dense biofilms, let alone achieve efficient gene regulation inside bacteria cells. Herein, an eye-drop system capable of penetrating biofilms and targeting bacteria for chemo-gene therapy in MRSA-caused bacterial keratitis is developed. This system employed rolling circle amplification to prepare DNA nanoflowers (DNFs) encoding MRSA-specific aptamers and mecR1 deoxyribozymes (DNAzymes). Subsequently, β-lactam antibiotic ampicillin (Amp) and zinc oxide (ZnO) nanoparticles are sequentially loaded into the DNFs (ZnO/Amp@DNFs). Upon application, ZnO on the surface of the nanosystem disrupts the dense structure of biofilm and fully exposes free bacteria. Later, bearing encoded aptamer, the nanoflower system is intensively endocytosed by bacteria, and releases DNAzyme under acidic conditions to cleave the mecR1 gene for PBP2a down-regulation, and ampicillin for efficient MRSA elimination. In vivo tests showed that the system effectively cleared bacterial and biofilm in the cornea, suppressed proinflammatory cytokines interleukin 1β (IL-1β) and tumor neocrosis factor-alpha (TNF-α), and is safe for corneal epithelial cells. Overall, this design offers a promising approach for treating MRSA-induced keratitis.

1. Introduction

Bacterial keratitis (BK) is a potentially vision-threatening eye infection that can lead to visual impairment or even blindness.[1] It is often caused by corneal trauma, wearing contact lenses, or the use of contaminated surgical instruments during ophthalmic procedures.[2] *Staphylococcus aureus* is the most common causative pathogen for bacterial keratitis, with ≈30% of cases attributed to methicillin-resistant *S. aureus* (MRSA). The MRMecR1 gene is a unique resistance gene in MRSA that encodes penicillin-binding protein PBP2a through the mecR1 signaling pathway.[3] PBP2a has a low affinity for β-lactam antibiotics and can catalyze cell wall synthesis even in the presence of β-lactam antibiotics, which contributes to its high level of antibiotic resistance.[4] Consequently, disrupting the mecR1 pathway is a promising strategy to restore the susceptibility of MRSA to β-lactam antibiotics by reducing PBP2a protein expression.

Oligonucleotide therapeutics can regulate target genes intracellularly by supplementing downregulated genes or

M. Ran, J. Yan, H. Zhang
Joint Centre of Translational Medicine
The First Affiliated Hospital of Wenzhou Medical University
Wenzhou, Zhejiang Province 325015, China
E-mail: Meixin.Ran@abo.fi; jiaqi.yan@abo.fi; hongbo.zhang@abo.fi

M. Ran, J. Yan, H. Zhang
Pharmaceutical Sciences Laboratory
Åbo Akademi University
Turku Bioscience Centre
University of Turku and Åbo Akademi University
Turku 20520, Finland

R. Sun, Y. Zhang
Department of Pharmaceutics
School of Pharmacy
Shenyang Pharmaceutical University Shenyang
Shenyang 110016, China
E-mail: sunr4021@163.com; zhangyu@syphu.edu.cn

A. T. Pulliainen
Institute of Biomedicine
Research Unit for Infection and Immunity
University of Turku
Kiinamyllynkatu 10, Turku FI-20520, Finland
E-mail: arto.pulliainen@utu.fi

The ORCID identification number(s) for the author(s) of this article can be found under https://doi.org/10.1002/smll.202304194

DOI: 10.1002/smll.202304194

silencing overexpressed genes, offering unique advantages compared to traditional drugs.[5] Deoxyribozymes (DNAzymes) are a type of oligonucleotide therapeutic agent based on single-stranded DNA.[6] Under the assistance of metal ions and following the base-pairing principle, they can specifically cleave target messenger RNA (mRNA) at certain sites without interfering with other cellular mechanisms. Compared to small interfering RNA (siRNA) and antisense nucleotides, DNAzymes show higher potential for clinical translation due to their superior stability, lower immunogenicity, and lower cost.[7]

Of note, researchers have already designed DNAzymes to inhibit the mecR1 gene,[8] which achieved sensitization therapy for planktonic MRSA to β-lactam antibiotics. However, even though DNAzymes have demonstrated the ability to effectively cleave target mRNA in vitro,[9] their potential gene therapy applications within bacteria still face several limitations. These include difficulties in achieving bacterial targeting, challenges in being taken up by bacteria, and the lack of sufficient cofactors within bacteria. In addition, 80% of bacterial infections are related to bacterial biofilm formation. Bacteria within biofilms exhibit different morphologies and physiological functions compared to planktonic bacteria, leading to a significantly increased antibiotic tolerance ranging from 10 to 1000 times.[10] Consequently, it is crucial to enhance the penetrability of DNAzymes into biofilms and achieve enhanced bacterial targeting and endocytosis.

The application of nanotechnology not only enhances the stability of gene drugs but also enables targeted delivery through modifications, thereby improving therapeutic efficacy.[11] Recently, the use of isothermal rolling circle amplification[12] (RCA)technology to prepare DNA nanoflower systems, equipped with various DNA functional components and metal ions has been widely developed in the field of cancer therapy. Inspired by this, we hypothesize to concatenate mecR1-specific DNAzymes and bacterial-targeting aptamers[13] to create a nanoflower system through RCA,[14] which is capable of targeting bacteria and silencing mecR1 mRNA. The nanoflowers are formed bases on DNA templates through magnesium phosphate precipitation, which can enable efficient DNAzyme-based gene regulation within bacterial cells, under acidic conditions with Mg^{2+} as co-factor. Additionally, zinc oxide (ZnO) nanoparticles, which are pH sensitive, low cytotoxic, well bioavailable, and biocompatible, are widely used to treat biofilm-associated infections by disrupting the biofilm.[15] Therefore, the incorporation of ZnO nanoparticles into the nanosystem will enhance its ability to penetrate the biofilm.

Drawing on the hypotheses discussed earlier, we have designed a functional DNA nanoflower eye-drop system, that integrated bacteria-targeting aptamer and mecR1-cleaving DNAzyme, for the treatment of MRSA-caused keratitis (as shown in **Scheme 1**). This system was simultaneously loaded with ZnO and β-lactam antibiotic ampicillin, abbreviated as ZnO/Amp@DNFs. Experimental results showed that when ZnO/Amp@DNFs nanoplatform was dropped into the eye, the released zinc oxide nanoparticles could first suppress the extracellular polymeric substance (EPS) of biofilm, and expose free bacteria. Subsequently, the aptamer-encoded DNA nanoflowers could recognize MRSA and be preferentially internalized by the bacteria. Under acidic conditions in the bacteria microenvironment, the nanoflower system released both Mg^{2+} ions and DNAzymes to form the activated gene-regulatory machinery, which silenced the mecR1 gene and ultimately restored the sensitivity of MRSA to β-lactam antibiotics. Both in vitro antibiofilm assays and in vivo animal experiments of bacterial keratitis have demonstrated the effectiveness of this nanoplatform for treating bacterial keratitis. Based on the programmable RCA assembly strategy, our DNAzyme nanoplatform design shows tremendous potential in developing multifunctional intelligent gene therapies for biofilm-associated bacterial keratitis.

2. Results and Discussion

To verify the cleavage ability of DNAzymes on MecR1 mRNA, a polyacrylamide gel electrophoresis (PAGE) experiment was first conducted (Figure S1, Supporting Information), and lane 1 was set as a DNA ladder. From the results, we found when DNAzymes (lane 2) incubated with substrate strand MecR1 mRNA (lane 3), a new and lagging band was generated (lane 4). However, due to the absence of a metal cofactor, no substrate strand was cleaved. Next, different concentrations of Mg^{2+} ions (0.1, 1, and 5 mM) were added to the system and we found that DNAzymes could efficiently cleave the MecR1 mRNA substrate (lanes 5, 6, and 7). During this process, the efficiency of cleavage increased with the concentration of metal ions. When the metal ion concentration reached 5 mM, the substrate was completely cleaved (lane 7). Therefore, this in vitro experiment demonstrated that DNAzymes are capable of cleaving the Mec-A mRNA.

To achieve targeted downregulation of antibiotic-resistant gene MecR1 mRNA within the bacteria, DNA nanoflowers (DNFs) material were prepared using the rolling circle amplification[16] method. The DNA template strand for RCA contained a DNAzyme sequence for MecR1 mRNA silencing and an aptamer sequence for MRSA targeting. As the total number of base pairs in the DNA template sequence exceeded 100 bp, which increased the risk of synthetic errors, we divided the RCR template DNA strand into two parts and designed two primers to initiate RCA with the help of phi29 enzyme (**Figure 1**a).

Subsequently, we validated the binding ability between the DNA template strand and the primers, as well as the DNFs formation, by using the PAGE method. As shown in Figure 1b, the four lanes on the right corresponded to two DNA template strands and two primers. When the four strands were incubated together (group 1+2+3+4), multiple staggered bands of DNA were observed, due to the binding between the template strands and the primers. Then, upon the addition of phi29 DNA polymerase for 6 h to form DNA nanoflowers (DNFs), we found that most of the DNA was retained at the top of the gel. These results indicated that DNFs were successfully synthesized, since as a nanomaterial, the DNFs cannot move inside the gel.

Afterward, we analyzed the morphology and elemental composition of the DNFs. Under transmission electron microscopy (TEM), we observed that the internal structure of the DNA nanoflowers was dense, while the surface appeared porous and loosely arranged. Scanning electron microscopy (SEM)[17] revealed that the surface of the DNFs exhibited a petal-like structure, with a diameter of ≈450 nm, which is consistent with the TEM results (Figure 1c). To further identify the components of the DNA nanoflower materials, we conducted an elemental analysis by using energy dispersive X-ray (EDS) (Figure 1d,e). As

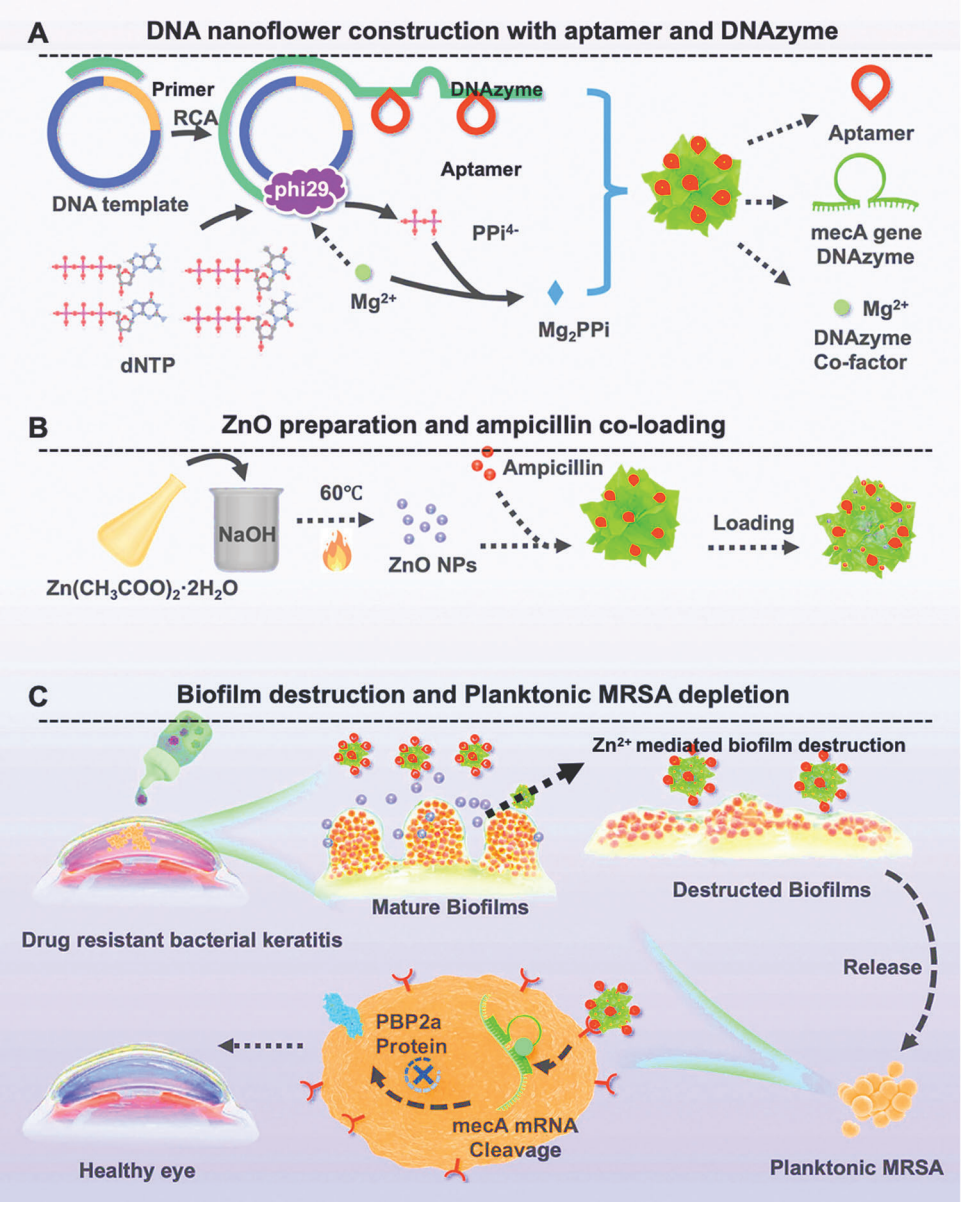

Scheme 1. Preparation process and mechanism of action of DNA nanoflower eye drops. A) Preparation process of DNA nanomaterials. B) Loading of zinc oxide and ampicillin. C) Bacterial clearance in keratitis.

DNA nanoflowers were formed by magnesium pyrophosphate sedimentation on the template DNA strand, we detected the presence of Mg elements in the DNA nanoflowers. Additionally, since DNA itself contains elements such as C, P, and O, we were also able to detect these elements in the DNA nanoflowers (Figure 1d,e).

Based on the aforementioned results, we have demonstrated the successful preparation of DNA nanoflower materials. However, numerous studies have shown that the size of nanomaterials can affect their antibacterial properties. Smaller nanoparticles have larger surface area-to-volume ratios, which increases the probability of contact with and penetration through the bacterial cell membrane.[18] Therefore, theoretically, we aim to prepare smaller DNFs to increase the efficacy of our nanoparticles. By controlling the RCA reaction time, we can regulate the size of the DNFs, and we found that the shorter the reaction time, the smaller the DNFs formed. However, through screening of reaction times (30 min, 1 h, 2 h, 4 h), we found if the reaction time is too short, the DNFs may not form completely and may not be able to load drugs (Figure 1f,g). When the reaction time was 2 h, the DNFs had an optimal morphology and smallest particle size of ≈130 nm base on TEM and dynamic light scattering (DLS) results, as shown in Figure 1h.

After verifying the successful preparation of DNA nanoflowers, the drug-loading capacity of DNFs was further tested. We incubated 100 μg of ampicillin with 100 μg of DNFs overnight and found that 100 μg of DNFs could load around 35 μg of ampicillin (abbreviated as Amp@DNFs), with a drug loading

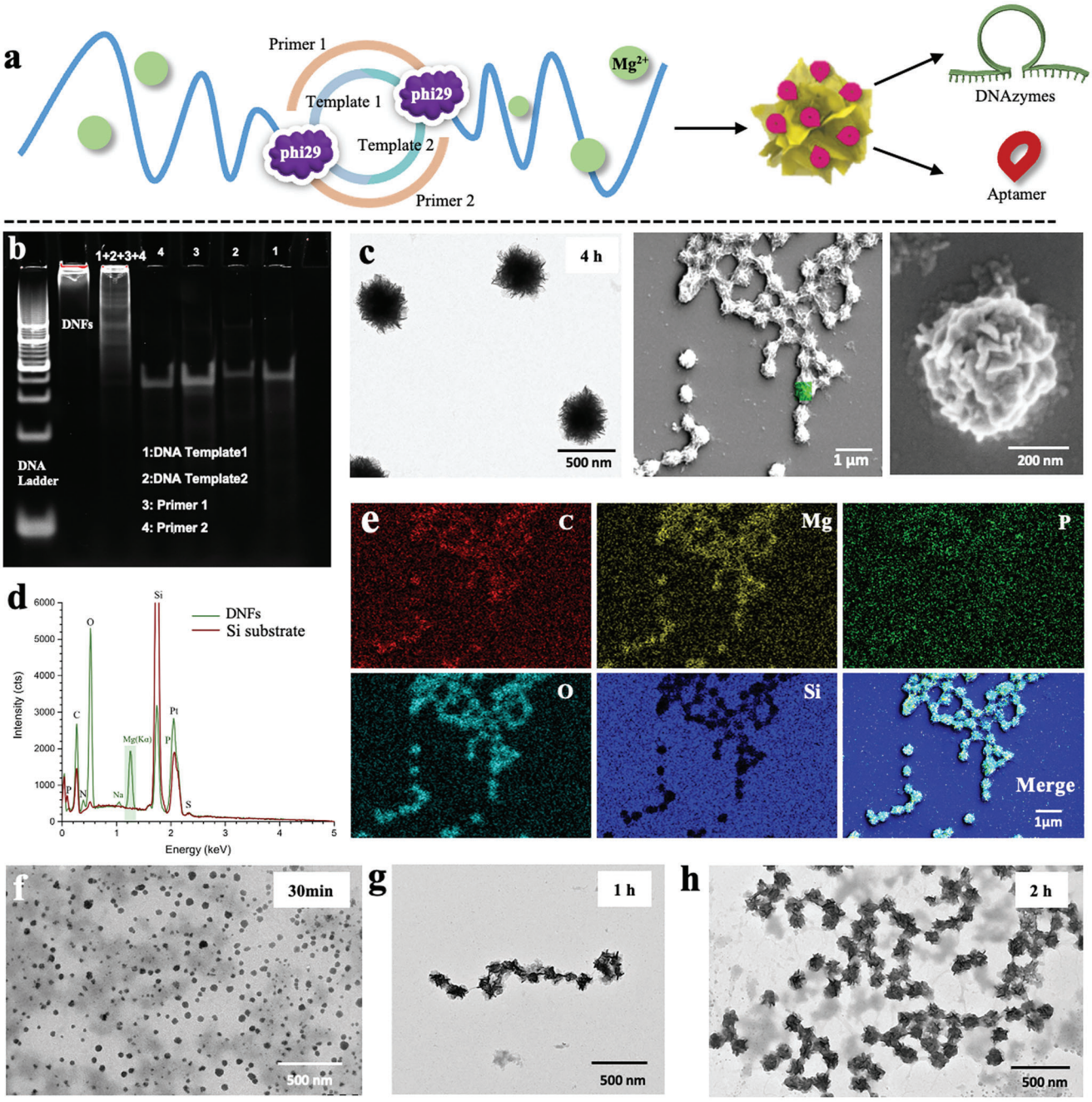

Figure 1. Preparation and characterization of DNA nanoflowers. a) Preparation of DNFs via RCA. b) Electrophoresis results of RCA reaction products on polyacrylamide gel. c) Characterization of DNFs obtained after 6 h of reaction time under transmission electron microscopy (TEM) and Scanning electron microscopy (SEM). d) Energy dispersive X-ray (EDS) spectrum of DNFs. e) EDS mapping of elements in DNFs. f) DNA nanoflowers obtained after 30 min of reaction time. g) TEM image of DNFs after 1 h RCA reaction. h) TEM image of DNFs after 2 h RCA reaction.

capacity as high as 25.9%. Due to the acidic pH in the microenvironment of biofilms[19] and the pH-sensitive degradation ability of DNA nanoflowers, we further investigated the pH-sensitive drug release ability of the Amp@DNFs system (Figure S2, Supporting Information). The results showed that within 12 h, the Amp@DNFs formulation could release over 80% of the Amp in a release medium with pH 5.0. However, only 20% of the drug was released in a release medium with a pH of 7.4. Therefore, the pH-responsive release of Amp within the Amp@DNFs system was confirmed.

Subsequently, we explored the synergistic antibacterial activity of Amp and ZnO nanoparticles on planktonic MRSA. The TEM result for ZnO was shown in **Figure 2**a, with the size around 5 nm. Theoretically, ZnO and ampicillin should have the potential for synergistic effects, since ZnO can inhibit biofilm formation and disrupt the bacterial cell wall, which can help ampicillin

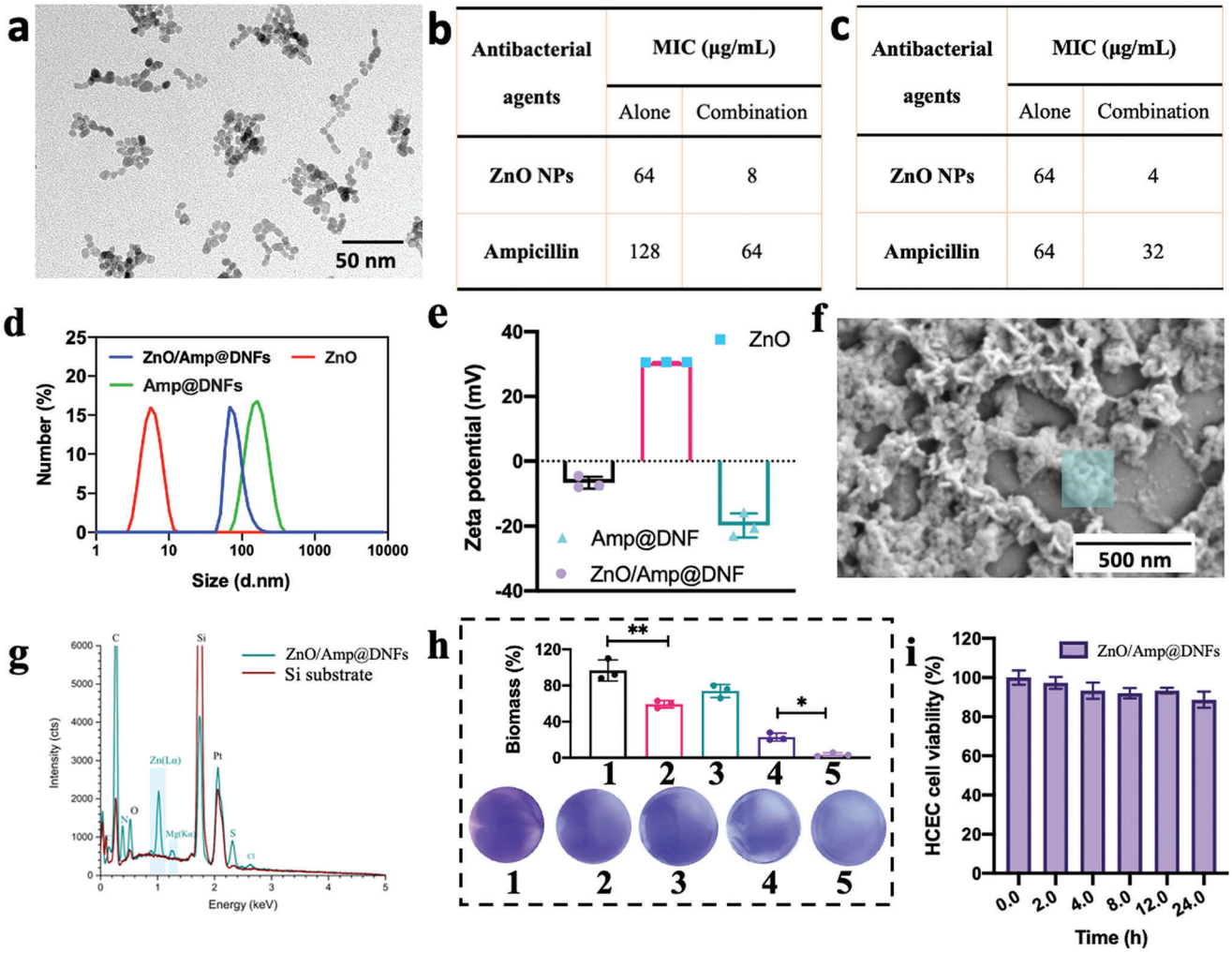

Antibacterial agents	MIC (μg/mL)	
	Alone	Combination
ZnO NPs	64	8
Ampicillin	128	64

Antibacterial agents	MIC (μg/mL)	
	Alone	Combination
ZnO NPs	64	4
Ampicillin	64	32

Figure 2. Synergistic effect of ZnO and Amp, as well as Amp@DNFs, and therapeutic efficacy and safety verification of the final formulation. a) TEM image of ZnO. b) Synergistic effect of ZnO and Amp. c) Synergistic effect of ZnO and Amp inside ZnO/Amp@DNFs system. d) Particle size of nanoparticles as determined by Dynamic Light Scattering (DLS). e) Nanoparticle potential. f,g) SEM image and EDS data of element analysis of the final formulation Amp/ZnO@DNFs. h) Antibiofilm experiments of each group against MRSA. i) Safety verification of the final formulation on human corneal epithelial cells. (*: $p < 0.05$, **: $p < 0.01$, $n = 3$).

inhibit the transpeptidase on the inner surface of the bacterial cell membrane. Upon experimental observation, it was found that the minimum inhibitory concentration (MIC) of ZnO nanoparticles and ampicillin exhibited a significant decrease when used in combination compared to their individual usage (Figure S3, Supporting Information and Figure 2b). The MIC values of ZnO NPs and ampicillin were measured to be 64 and 128 μg mL^{-1}, respectively. However, upon co-administration, the MIC of ZnO was found to reduce to 8 μg/mL and the MIC of ampicillin was reduced to 64 μg mL^{-1}.

However, when the Amp and ZnO are loaded into nanoparticles as ZnO/Amp@DNFs, they will undergo sustained-release processes. Therefore, we further investigated the synergistic therapeutic effect of ZnO and Amp inside the ZnO/Amp@DNFs system (Figure S4, Supporting Information). From the results, the DNFs carrier enhanced the therapeutic effect of Amp, reducing its MIC value to 64 μg mL^{-1}. Moreover, upon administration of ZnO/Amp@DNFs, the MIC values of ZnO and Amp decreased to 4 and 32 μg mL^{-1}, respectively (Figure 2c). Therefore, in the subsequent anti-biofilm experiments, 4 μg mL^{-1} of ZnO and 32 μg mL^{-1} of Amp were selected as the treatment concentration.

After obtaining the MIC treatment concentration, we characterized the final formulation ZnO/Amp@DNFs. It was reported that when smaller metal nanoparticles are loaded into the interior of DNFs, the nanoflowers can be compressed to form a more compact structure.[20] Therefore, after loading ZnO into DNA nanoflowers, the particle size of Amp@DNFs nanoparticles decreased from over 130 nm to around 95 nm (Figure 2d). In addition to changes in particle size, we also observed changes in the electric potential of the DNFs before and after ZnO addition (Figure 2e). We found that the DNFs had a negative potential of approximately −20 mV, but after adding ZnO NPs (about +30 mV) into the DNFs, the potential of the ZnO/Amp@DNFs shifted to −6 mV, indicating that the ZnO NPs were successfully loaded into the DNFs. Moreover, we also conducted elemental

analysis on the Amp/ZnO@DNF NPs (Figure 2f,g). We found that, in addition to magnesium, a large amount of zinc was detected inside the ZnO/Amp/DNFs nanoparticles, which proved further evidence of successful ZnO loading.

After demonstrating the successful preparation of ZnO/Amp/@DNFs, we further investigated its MRSA targeting ability. As nanoparticles have limited residence time at the infection site in a real physiological environment during eye drop treatment, we evaluated the interaction between nanoparticles and bacteria after short-term exposure (1 h), and the NPs were loaded with Cy3 dye. After incubation, the NP-bacteria complexes were centrifuged and washed with PBS to remove unbound NPs. The mixture was then resuspended in PBS buffer and the ability of NPs to specific target bacterial cells was detected by centrifugation, imaging, and flow cytometry. MRSA aptamer incorporate NPs showed significantly higher Cy3 fluorescence intensity (>4 times higher) compared to groups without aptamer modification (Figure S5, Supporting Information). These data suggest that the MRSA aptamer significantly enhances the binding ability of ZnO/Amp/@DNFs to the target bacteria.

Next, the biofilm inhibition ability of ZnO/Amp/@DNFs was tested by using the crystal violet staining method. The experiment included a blank group, Amp group, ZnO group, Amp+ZnO group, and the final formulation ZnO/Amp@DNFs group, each corresponding to numbers 1 to 5, as shown in Figure 2h. Crystal violet was diluted with ethanol and its absorbance peak was recorded at 590 nm. The results showed that compared to the blank group, the co-administration of ZnO and Amp could remove around 80% of the biofilm, while the final formulation group could remove more than 96% of the biofilm. These results demonstrated the inhibitory effect of the ZnO/Amp@DNFs on biofilm. Additionally, human corneal epithelial cells (HCEC) were also used to verify the safety of the final formulation on the cornea, and the results showed that ZnO/Amp@DNFs did not exhibit significant toxicity to HCEC cells within 24 h (Figure 2i). Therefore, ZnO/Amp@DNFs have specific bactericidal and biofilm-inhibiting capabilities.

To further analyze the inhibitory effects of the ZnO/Amp@DNFs on biofilms, we conducted a live/dead staining analysis using SYTO 9/propidium iodide (PI) fluorescence staining method, under confocal laser scanning microscopy. SYTO 9 emits green fluorescence, while PI emits red fluorescence, allowing for visualization of the status of MRSA within the biofilm (**Figure 3**a). The results reflected that Amp or ZnO alone can inhibit bacterial activity to some extent, but the combination between ZnO and Amp greatly enhanced the inhibition of MRSA. Furthermore, with the help of DNFs, ZnO/Amp@DNFs demonstrated the strongest bactericidal ability (Figure 3a). Based on the image in Figure 3a, the COMSTAT 2.1 program in the ImageJ plugin[21] was used to quantitatively analyze the average diffusion distance index (Figure 3d). The average diffusion distance (ADD) represents the distance of diffusion between the nutrient sources and the microorganisms in the biofilm.[22] The lower the numerical index, the lower the distance at which the bacteria in the biofilm obtain nutrient sources, indicating a smaller number of bacteria. From the results, it can be observed that a single treatment of Amp or ZnO reduced the average diffusion distance[23] by ≈50% and 20%, respectively. When Amp and ZnO were combined, the ADD was reduced by ≈75%. Furthermore, with the assistance of DNFs, the inhibition rate of ZnO/Amp@DNFs on ADD reached 84%, and the ADD was only about 0.03 μm, which demonstrated the inhibitory effect of ZnO/Amp@DNFs on biofilms (Figure 3d).

Afterward, as shown in Figure 3b, the inhibitory effect of the ZnO/Amp@DNFs nanoplatform on biofilm was further observed by obtaining colony-forming units (CFUs). The corresponding quantitative histogram of bacterial survival rate was generated by calculating the CFU amount divided by the control group CFU amount (Figure 3e). The survival rate results showed that the nanoflower system could inhibit about 98% of bacterial colony formation, which was much higher than the inhibition ability observed with the combination group of Amp and ZnO (about 80%), demonstrating its strong antibacterial ability.

In addition, the morphology and structure of bacteria under each treatment group were further characterized by transmission electron microscopy (TEM) (Figure 3c). Compared to the blank control group, bacteria treated with Amp and ZnO showed more cytoplasmic aggregations with numerous cell contents loss. When Amp and ZnO were used in combination, we found that some bacterial cell walls showed signs of dissolution. However, under the mediation of DNFs, a large number of bacteria in the ZnO/Amp@DNFs group showed cell wall dissolution, with contents aggregated and leaked. These results revealed the inhibitory effect of the ZnO/Amp@DNFs nanoplatform on MRSA.

To demonstrate the inhibitory effect of the DNA nanoflower material on the PBP2a protein expression inside bacteria, western blotting was performed (Figure 3f). The results showed that neither Amp nor ZnO nanoparticles could reduce the expression of PBP2a protein, whether used alone or in combination. However, when the ZnO/Amp@DNFs nanosystem was introduced, the expression of PBP2a protein inside bacteria was significantly down-regulated. Therefore, these results demonstrated the regulatory effect of the DNFs system on the drug-resistant gene expression of bacteria.

Encouraged by the excellent antibacterial performance of ZnO/Amp@DNFs, we further carried out its in vivo therapeutic effect through a rabbit model of BK infection. The rabbits were randomly divided into five groups, including the control group, ZnO group, Amp group, ZnO+Amp group, and ZnO/Amp@DNFs group. As shown in **Figure 4**a, 5 μL MRSA (1000 CFU) was injected into the rabbit cornea using an injection method to construct the BK model. The formed rabbit cornea exhibited signs of corneal opacity, photophobia, eyelid tearing, redness, and increased secretion. Subsequently, the rabbits were treated according to different groups and were observed and photographed daily to assess the severity of infection based on the level of bacterial keratitis. After treatment, the rabbits were sacrificed and their corneas were dissected for subsequent biochemical experiments. In addition, the DNF (drug-loaded nanoformulation) nanomaterials are encapsulated in 1.5 mL Eppendorf tubes in doses required for daily use, followed by freeze-drying. These tubes are then stored at 4 °C.

In Figure 4a, the control group (1) showed gradually worsening infection of the cornea after 12 days, with corneal opacity, congestion, edema, and exudation with abundant neovascularization. In contrast, the ZnO+Amp group (4) showed better therapeutic effects than either ZnO (3) or Amp (2) monotherapy, with slight

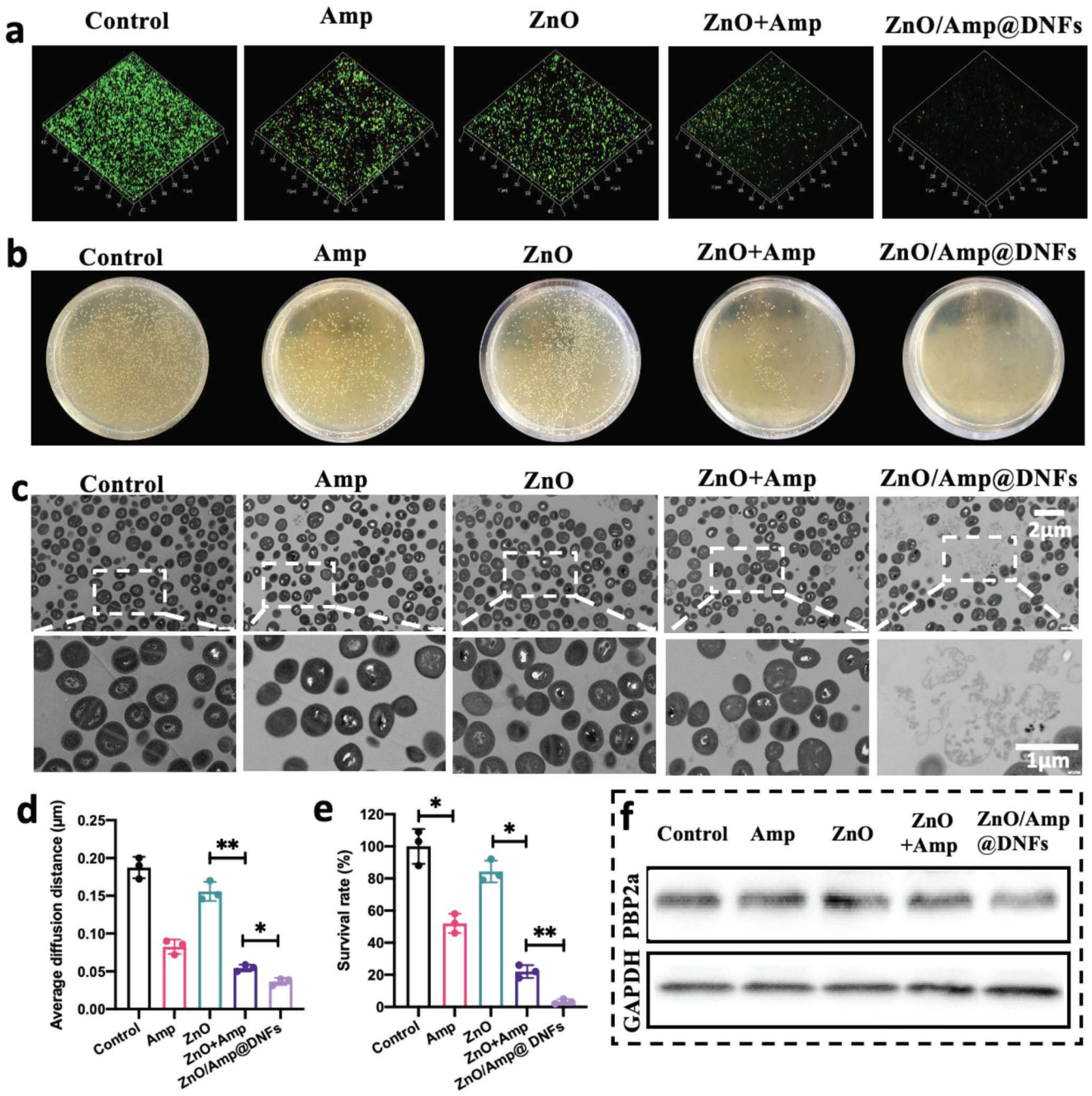

Figure 3. Antimicrobial experiments and bacterial morphology characterization. a) Confocal laser scanning microscopy images of MRSA stained with SYTO 9/propidium iodide (PI). b) Bacterial agar plate culture. c) TEM characterization of bacterial morphology. d) Diffusion distance between bacteria and nutrient substances in confocal microscopy images. e) Bacterial survival rate in agar plate culture. f) Bacterial protein expression level. (*: $p < 0.05$, **: $p < 0.01$, $n = 3$).

relief of corneal conditions and gradual disappearance of some opacity and edema. After treatment with ZnO/Amp@DNFs, the cornea became transparent, inflammation was effectively controlled, and there was almost no new blood vessel formation. Moreover, the clinical grading score of the ZnO/Amp@DNFs treatment group (grade 1: Clinical action rarely required) was also greater than the ZnO+Amp group (grade 3: Moderate, clinical action usually required) (Figure 4d).

Furthermore, the results of the corneal scoring showed that rabbits treated with ZnO/Amp@DNFs had the lowest level of corneal infection and the clearest corneas upon dissection, with relatively low levels of opacity, demonstrating improvement in light transmission (Figure 4b). On the 12th day, the cornea in the ZnO/Amp@DNFs treatment group had almost fully recovered, with a corneal ulcer area of about 2 mm^2, compared with the ZnO+Amp group of about 16 mm^2 (Figure 4e).

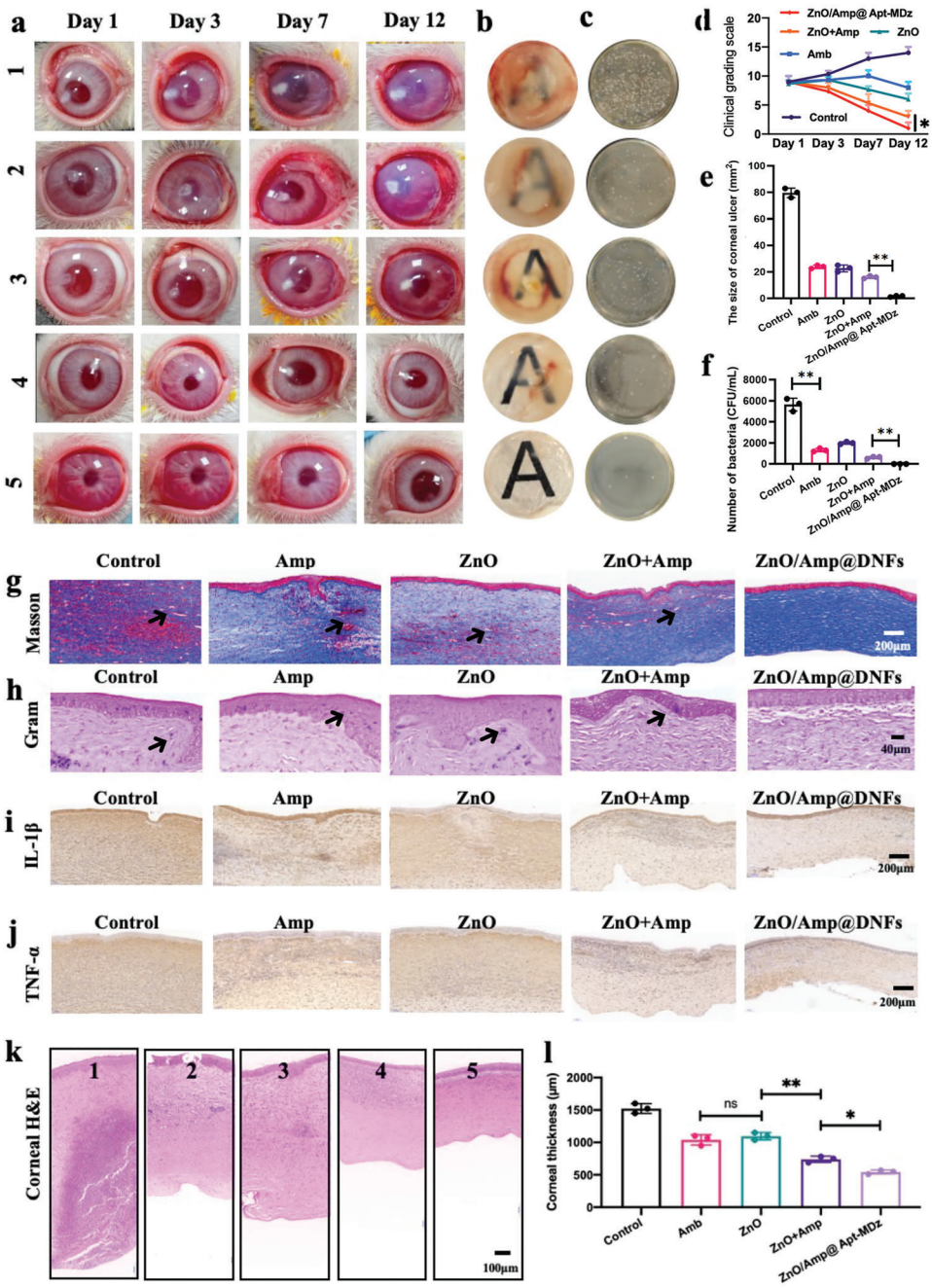

Figure 4. In vivo therapeutic experiment of DNA nanoflower-based therapy for bacterial keratitis. The figure includes a) antibacterial experiment photos of the cornea, b) comparison photos of corneal transparency (ulcer area), c) bacterial colony experiment after cornea extraction, d) clinical score photos of antibacterial effect on the cornea, e) quantitative measurement of corneal ulcer area, f) quantitative measurement of bacterial colony count, g) Masson trichrome staining experiment (black arrow represents blood vessels), h) Gram staining experiment of bacteria (black arrow represents bacteria), i,j) immunohistochemistry experiment of pro-inflammatory cytokines IL-1β and TNF-α, k,l) corneal thickness characterization and quantitative analysis. (*: $p < 0.05$, **: $p < 0.01$, $n = 3$). 1: Control, 2: Amp; 3: ZnO; 4: Amp+ZnO; 5: ZnO/Amp@DNFs.

Additionally, MRSA bacteria were collected from corneal tissues for plate culturing 10 days after treatment. Compared to other groups, ZnO/Amp@DNFs showed significantly fewer colonies (Figure 4c,f). The above results demonstrate from a macroscopic perspective the inhibitory ability of the DNA nanoflower system against corneal bacteria. It can simultaneously achieve bacterial clearance and improvement of ocular inflammation symptoms.

In addition, we further evaluated the therapeutic effects of different treatments on bacterial keratitis from a pathological and histological perspective, including antimicrobial and

anti-inflammatory effects. Firstly, Masson's trichrome staining was used to evaluate the structure of corneal stromal collagen, as shown in Figure 4g, where blue represents collagen fibers and purple/red represents blood vessels (black arrow). The control group showed irregular lamellar structure with severe corneal edema. The Amp and ZnO combination group exhibited a more orderly collagen fiber arrangement, but blood vessels still appeared in large numbers. In the ZnO/Amp@DNFs treatment group, a neat blue arrangement was observed with almost no blood vessels, indicating that ZnO/Amp@DNFs can significantly alleviate the bacterial-induced disruption of collagen and changes in the structural arrangement.

Then, Gram staining of tissue sections (Figure 4h) showed that there were dark purple clusters in the corneal stroma of the Amp or ZnO treatment group, indicating the presence of MRSA. However, in the Amp and ZnO combination group, there were almost no bacteria marked with dark purple (black arrow) in the stromal layer. Encouragingly, in the ZnO/Amp@DNFs group, there were no dark purple clusters present in either the corneal surface or the stromal layer, indicating that the ZnO/Amp@DNFs nanomedicine can completely achieve bacterial clearance.

The results in Figure 4i,j show that the control group exhibited severe infiltration of pro-inflammatory cytokines (IL-1β, TNF-α) and a significant increase in corneal thickness. The expression of inflammatory factors was reduced when Amp or ZnO was used alone, but the treatment effect was not as significant as that of the combination treatment with Amp and ZnO. It is worth noting that the ZnO/Amp@DNFs group showed almost no expression of inflammatory factors, indicating that the nanoflower system can effectively inhibit the inflammatory response in bacterial keratitis. In addition, the corneal thickness is shown in Figure 4k,l. The corneal thickness of the control group was about 1500 μm. After treatment with Amp or ZnO alone, the corneal condition was slightly improved, with a thickness of about 1000 μm. After treatment with Amp and ZnO in combination, the inflammatory response was effectively controlled, and the corneal thickness was significantly reduced to about 700 μm. Of note, in these treatments, the ZnO/Amp@DNFs treatment group had a corneal thickness that returned to normal, at only about 500 μm. Therefore, the above results indicate that DNFs can effectively enhance the combination therapy of Amp and ZnO, and are an effective antibacterial system for treating bacterial keratitis.

Furthermore, the biocompatibility of ZnO/Amp@DNFs eye drops, such as preliminary toxicity and the effect on eye function were assessed by administering them to healthy rabbit eyes for 7 days. The results showed that there were no significant changes in the corneal epithelial defect area of healthy rabbits treated with ZnO/Amp@DNFs under both white light and cobalt blue light (**Figure 5**a). The H&E staining images (Figure 5b) revealed that there was no significant difference in the structure and thickness of the cornea, conjunctiva, and retina between infected and healthy eyes after treatment with ZnO/Amp@DNFs.

In addition, we further tested the tear secretion function of rabbit eyes. The wetting length of fluorescein was similar in healthy eyes, and healthy eyes treated with ZnO/Amp@DNFs, which were around 14 mm (Figure 5c,d). However, the length of the tear fluorescence strip in the control group was significantly shortened (around 7 mm), indicating the occurrence of dry eye symptoms. After treatment with ZnO/Amp@DNFs, the infected eyes showed a recovery in tear secretion function, without any significant effect on healthy eyes.

Overall, these preliminary toxicity test results suggested that ZnO/Amp@DNFs eye drops do not cause local toxicity and can induce the recovery of tear secretion function in infected rabbit eyes. These findings indicated that ZnO/Amp@DNFs eye drops may be a promising option for treating eye infections.

3. Conclusion

In conclusion, we have successfully developed a highly effective antibacterial strategy based on ZnO/Amp@DNFs, which has demonstrated great potential in eradicating MRSA and its biofilm. The RCA-powered nanoflower system offers a powerful tool for amplifying mecR1 mRNA-cleaving DNAzymes and MRSA-targeting aptamers while providing the necessary cofactors to greatly enhance their therapeutic efficacy. Meanwhile, the released ZnO had an inhibitory effect on EPS and enhanced the penetration ability of the biofilm. The exposed bacteria combined with the aptamer of ZnO/Amp@DNFs to enhance the endocytosis of nanoparticles. In both in vivo and in vitro studies, ZnO/Amp@DNFs were found to suppress PBP2a expression, downregulate IL-1β and TNF-α inflammatory factors, and exhibit negligible toxicity. The use of a nano-droplet formulation may also reduce dosing frequency and treatment burden. Overall, our findings suggest that ZnO/Amp@DNFs have significant potential for clinical applications in the treatment of bacterial infections, providing a novel approach to combat antibiotic-resistant bacteria and improve patient outcomes. For future prospects, we believe that the incorporation of photosensitizing agents into the nucleotide substrates used in rolling circle amplification can significantly enhance the therapeutic efficacy of DNA nanoflowers (DNFs). This strategy enables DNFs to acquire photodynamic therapy (PDT) capabilities. By combining the targeted delivery of DNFs with the photodynamic eradication of neovascularization, this approach will show immense potential for achieving groundbreaking treatment outcomes.

4. Experimental Section

Synthesis of DNA Nanoflowers: To avoid synthesis errors in DNA sequences longer than 100 bases, the template strand was fragmented into two pieces (T1 and T2). Then, based on the template strand, primer strands P1 and P2 were designed for the both-end ligation of T1 and T2 into a circular template. Linear template strands (T1 and T2, 2 μM each) and primer strands (P1 and P2, 4 μM each) were heated in a ligase reaction buffer at 95 °C for 5 min and slowly cooled to room temperature over a period of more than 3 h (≈0.5 °C min^{-1} cooling rate). Subsequently, gaps in the hybridized DNA were closed by T4 ligase (20 U μL^{-1}) through overnight incubation at 16 °C, followed by heating at 65 °C for 10 min to terminate the enzyme reaction. To remove excess primer strands, the ligated template DNA was incubated with exonuclease I (480 mU μL^{-1}) in a reaction buffer at 37 °C for 3 h, followed by incubation at 80 °C for 15 min to heat-terminate the enzyme reaction. For a single RCA reaction, circular DNA template strands and dNTPs (1 mM) were combined with recombinant albumin, phi 29 reaction buffer, and phi 29 polymerase (1 U μL^{-1}), and heated at 30 °C for different reaction times (30 min, 1 h, 2 h, 4 h). The RCA reaction was terminated by heating at 75 °C for 10 min. Then NFs were washed with water without ribozyme, centrifuged and precipitated, and stored at 4 °C for future use.

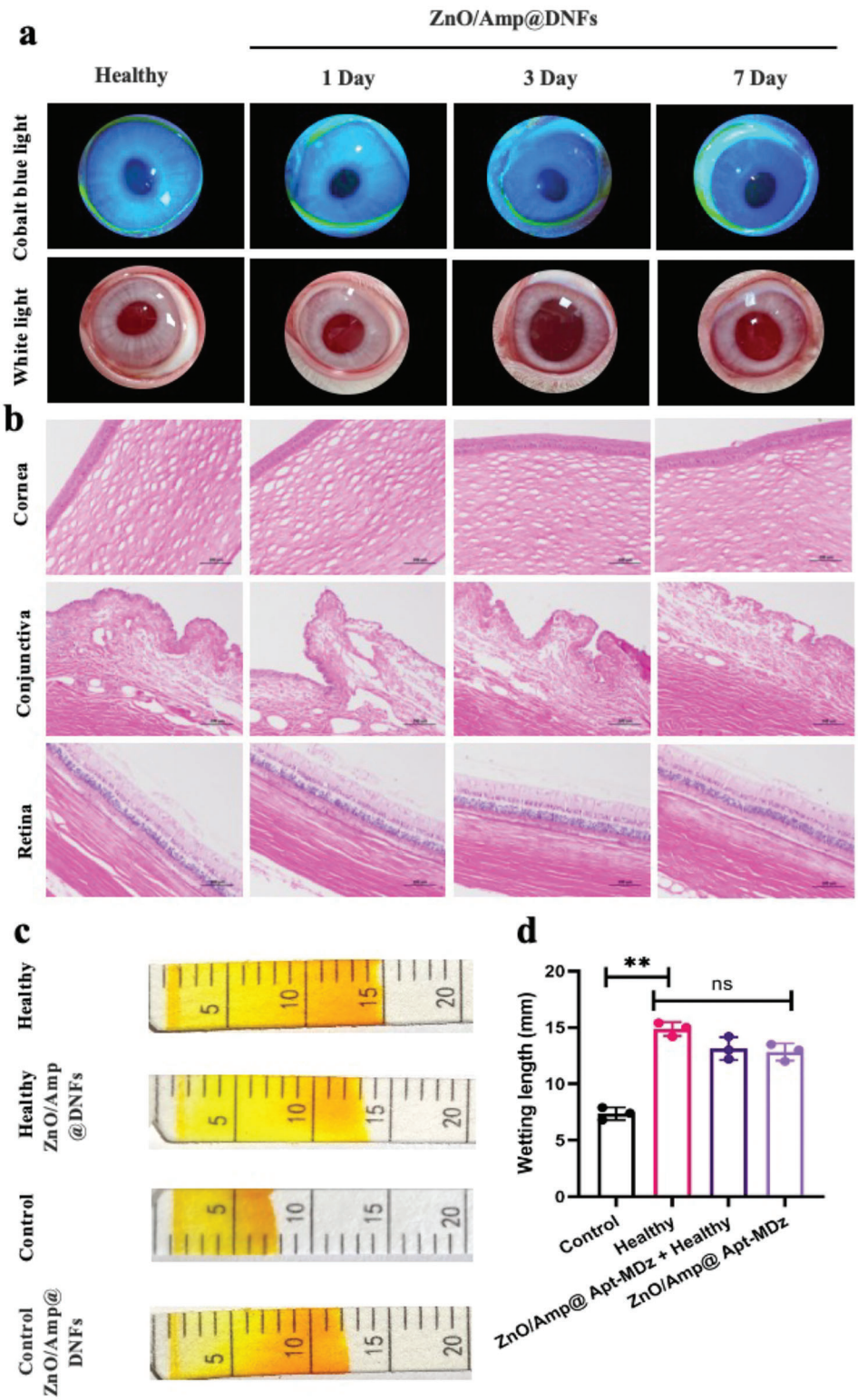

Figure 5. Biosafety and irritation test of the eye with ZnO/Amp@DNFs eye drops. a) Sodium fluorescein staining of healthy corneas with or without ZnO/Amp@DNFs treated on days 1, 3, and 7. ZnO/Amp@DNFs nanoparticles (40 μg mL^{-1}, $n = 3$). b) Histological examination of the cornea, conjunctiva, and retina of Healthy, ZnO/Amp@DNFs treated on days 1, 3, and 7, ($n = 3$). c) Sodium fluorescein thread measurement by Schiemer tear test strips. d) Quantitative analysis of wetting length of control, healthy, ZnO/Amp@DNFs+healthy, and ZnO/Amp@DNFs treated groups. (*: $p < 0.05$, **: $p < 0.01$, $n = 3$).

Synthesis of ZnO: The synthesis procedure of ZnO nanoparticles was conducted as follows: First, 3.73 mmol of zinc acetate was added to 40 mL of anhydrous ethanol and heated to 70 °C until fully dissolved under vigorous stirring. Next, 7.22 mmol of sodium hydroxide was dissolved in 25 mL of refluxing ethanol in a separate flask. Both solutions were cooled in an ice bath before slowly adding the sodium hydroxide solution into the solution containing zinc acetate. The mixture was stirred for 2 h at 60 °C, resulting in the precipitation of ZnO nanoparticles. The precipitates were collected and washed thrice with anhydrous ethanol using ultrasonication, followed by vacuum drying at room temperature to obtain the final ZnO nanoparticles.

MIC Values Testing for ZnO/Amp@DNFs for Anti-Free MRSA Experiments: The synergistic effect for ZnO and Amp were tested by combining two therapeutic agents directly, or after loading into the DNA nanoflowers. For the MIC values testing of ZnO NPs and ampicillin, different concentration of ZnO (0, 1, 2, 4, 8, 16, 32, and 64 μg mL^{-1}) was combined with Ampicillin (0, 0.5, 1, 2, 4, 8, 32, 64, 128, 256, and 512 μg mL^{-1}) for synergistic therapy. For MIC testing of ZnO NPs and ampicillin after being loaded inside the DNFs, different amounts of Amp and ZnO were loaded inside the DNFs. For Amp, the concentration was 0, 0.5, 1, 2, 4, 8, 32, 64, 128, 256, and 512 μg mL^{-1}, and for ZnO, the concentration was 0, 1, 2, 4, 8, 16, 32, and 64 μg mL^{-1}.

Preparation of ZnO/Amp@DNFs for Antibiofilm Experiments: ZnO/Amp@DNFs were synthesized by adding an additional 32 μg Amp and 4 μg of ZnO nanoparticles to 100 μg DNFs. The obtained product was washed with ultrapure water and centrifuged at 8000 rpm for 15 min for a total of three times. The nanoparticles were then redispersed multiple times by ultrasonication and suction.

Analysis of Native Polyacrylamide Gel Electrophoresis (PAGE): Different samples (T1, T2, P1, P2, T1+T2+P1+P2, DNFs) and a super low range DNA ladder (ranging from 10 to 300 bp) were loaded into an 18% native PAGE gel and run at a constant voltage of 100 V in 1× TBE running buffer for 1.5 h. After staining with GelRed for 5 min, images were obtained using the GelDoc Go gel imaging system (Bio-Rad) at an excitation wavelength of 365 nm.

Characterization of DNFs and ZnO/Amp@DNFs: To study the morphology and elemental distribution, DNFs were imaged by a field-emission SEM (FE-SEM) with EDS. In addition, a JEM-1400 Plus transmission electron microscope (TEM) was also employed for DNFs examination at 80 kV voltage. The hydrodynamic diameter and zeta potential of DNFs were obtained using a Zetasizer Nano ZS instrument (Malvern, UK).

Target Ability of ZnO/Amp@DNFs to MRSA: MRSA was incubated with the aptamer-modified and unmodified ZnO/Amp@DNFs loaded with cy3 for 1 h, and then the bacterial-nanoparticle complex was harvested, which was photographed after gentle centrifugation. In addition, the uptake of MRSA was analyzed by flow cytometry, and the fluorescence intensity was analyzed. The excitation wavelength of cy3 is 488 nm and the maximum emission wavelength is 570 nm.

Antibacterial Analysis Against Biofilms: Biofilms established for 24 h were treated with different preparation groups (control, ZnO, Amp, ZnO+Amp, ZnO/Amp@DNFs) and incubated with nanoparticles for 12 h. The dead bacteria on the biofilm surface were then washed off with PBS, and the biofilms were collected and spread on agar plates and incubated at 37 °C under aerobic conditions for 24 h. The number of bacterial cells was calculated by counting all colonies on the agar plates.

Morphological Characterization: After treating MRSA with different groups (control, ZnO, Amp, ZnO+Amp, ZnO/Amp@DNFs), bacteria were collected by centrifugation. Then, the bacteria were fixed, dehydrated, permeabilized, embedded, ultrathin sectioned, stained, and observed under JEM-1400 Plus TEM.

Establishment of the BK Model and Therapeutic Strategy: The animal experimentation was approved by the University Ethics Committee of Shenyang Pharmaceutical University (license number: SYPU-IACUC-2022-1224-401). 15 Japanese white rabbits were randomly divided into five groups, with three rabbits in each group. Under sterile conditions, 5 μL of MRSA (ATCC 43300) containing 1000 colony-forming units (CFU) was injected into the corneal stroma of both eyes of the rabbits to establish an experimental bacterial keratitis (BK) model. After 24 h of inoculation, the rabbits' eyes were examined under a slit-lamp microscope and scored for corresponding indicators: clinical observation indicators including secretion, stromal infiltration, and stromal edema, with each observation indicator scored on a scale of 0 to 4 according to the severity. Rabbits with similar levels of inflammation were selected for further experimental research. Then, rabbits were treated with control, ZnO, Amp, ZnO+Amp, and ZnO/Amp @ DNFs via topical instillation respectively three times one day.

The anterior segment morphology was observed using slit lamp biomicroscopy on days 1, 3, 7, and 12, and scored based on the four indicators mentioned above (0–16 points). On day 12, the rabbits were euthanized, and their corneas were removed and photographed for overall appearance and clarity evaluation. The size of the ulcer area was analyzed using ImageJ software.

The excised corneas were homogenized in 1.0 mL sterile PBS using a KZ-II Tissue homogenizer (Wuhan Servicebio Technology Co., Ltd.). After high-speed centrifugation (10 000 g, 10 min), the supernatant was diluted 20 times with LB medium, and 100 μL of the diluted solution was used for MRSA selection medium agar plates. The number of colonies grown on the plate after overnight incubation at 37 °C represented the live bacterial density (CFU mL^{-1}) ($n = 3$). After 12 days of treatment, tissue specimens were collected and fixed in 4% paraformaldehyde for histopathological analysis (H&E, Masson staining, gram staining) and immunohistochemical analysis (TNF-α, IL-1β).

Biosafety of ZnO/Amp@DNF: After treating for 1, 3, and 7 days in vivo, 0.5% fluorescein sodium (2 μL) was added to the cornea to stain the corneal epithelial defects. Fluorescent images were captured in the cobalt blue channel using a slit-lamp imaging system and quantified using ImageJ software. On the 12th day, a 30 mm long Schiemer tear test strip was placed in the inferior fornix of rabbit eyes for 30 s. When the fluorescein sodium line comes into contact with tears, the color changes from orange to yellow.

Supporting Information

Supporting Information is available from the Wiley Online Library or from the author.

Acknowledgements

M.R., R.S., and J.Y. contributed equally to this work. This work was supported by the Research Fellow (Grant No.353146), Project (347897), Solution for Health Profile (336355), InFLAMES Flagship (337531) grants, and (295296) from Academy of Finland, Finland China Food and Health International Pilot Project funded by the Finnish Ministry of Education and Culture. National Natural Science Foundation of China [82172086], National Key R&D Program of China [2020YFE0201700], Shenyang Science and Technology Talent Support Program [RC210447], Career Development Program for Young and Middle-aged Teachers of Shenyang Pharmaceutical University [ZQN2019004], Meixin Ran (CSC202207960005) and Jiaqi Yan (CSC202107960001) were sponsored by the China Scholarship Council.

Conflict of Interest

The authors declare no conflict of interest.

Data Availability Statement

The data that support the findings of this study are available in the supplementary material of this article.

Keywords

biofilms, DNA nanoflower, DNAzymes, gene therapy, methicillin-resistant *Staphylococcus aureus*

Received: May 18, 2023
Revised: June 28, 2023
Published online: July 25, 2023

[1] a) H. Han, Y. Gao, M. Chai, X. Zhang, S. Liu, Y. Huang, Q. Jin, A. Grzybowski, J. Ji, K. Yao, *J. Controlled Release* **2020**, *327*, 676; b) Y. Sun, W. Zhang, M. Wang, H. Liu, Q. Li, J. Luo, M. Zhao, S. Liu, X. Wang, *Nano Res.* **2022**, *16*, 849; c) J. He, Y. Ye, D. Zhang, K. Yao, M. Zhou, *Adv. Mater.* **2022**, *34*, 2206437.

[2] a) H. J. Jian, R. S. Wu, T. Y. Lin, Y. J. Li, H. J. Lin, S. G. Harroun, J. Y. Lai, C. C. Huang, *ACS Nano* **2017**, *11*, 6703; b) Y. Qiao, J. He, W. Chen, Y. Yu, W. Li, Z. Du, T. Xie, Y. Ye, S. Y. Hua, D. Zhong, K. Yao, M. Zhou, *ACS Nano* **2020**, *14*, 3299.

[3] Z. Hou, Y. Zhou, H. Wang, H. Bai, J. Meng, X. Xue, X. Luo, *Arch. Med. Sci.* **2011**, *7*, 414.

[4] a) A. Rajabiani, F. Kamrani, M. A. Boroumand, H. Saffar, *Jundishapur J. Microbiol.* **2014**, *7*, 9181; b) C. Santiago, E. L. Pang, K. H. Lim, H. S. Loh, K. N. Ting, *BMC Complementary Altern. Med.* **2015**, *15*, 178.

[5] a) J. Yan, H. Zou, W. Zhou, X. Yuan, Z. Li, X. Ma, C. Liu, Y. Wang, J. M. Rosenholm, W. Cui, X. Qu, H. Zhang, *Biomater. Sci.* **2022**, *10*, 4119; b) C. Pacheco, A. Baião, T. Ding, W. Cui, B. Sarmento, *Adv. Drug Delivery Rev.* **2023**, *194*, 114724; c) X. Huang, N. Kong, X. Zhang, Y. Cao, R. Langer, W. Tao, *Nat. Med.* **2022**, *28*, 2273; d) X. Huang, C. Liu, N. Kong, Y. Xiao, A. Yurdagul, I. Tabas, W. Tao, *Nat. Protoc.* **2022**, *17*, 748; e) N. Kong, R. Zhang, G. Wu, X. Sui, J. Wang, N. Y. Kim, S. Blake, D. De, T. Xie, Y. Cao, W. Tao, *Proc. Natl. Acad. Sci. U. S. A.* **2022**, *119*, 2112696119; f) Y. Xiao, Z. Tang, X. Huang, W. Chen, J. Zhou, H. Liu, C. Liu, N. Kong, W. Tao, *Chem. Soc. Rev.* **2022**, *51*, 3828.

[6] J. Yan, M. Ran, H. Zhang, *Biomed. Technol.* **2023**, *4*, 21.

[7] J. Yan, M. Ran, X. Shen, H. Zhang, *Adv. Mater.* **2023**, 2300374.

[8] Z. Hou, J. R. Meng, C. Niu, H. F. Wang, J. Liu, B. Q. Hu, M. Jia, X. X. Luo, *Clin. Exp. Pharmacol. Physiol.* **2007**, *34*, 1160.

[9] B. C. Wong, J. Abu Bakar, A. Dhanoa, H. S. Tan, *Curr. Genet.* **2022**, *68*, 27.

[10] a) L. Tian, K. Jackson, M. Chan, A. Saif, L. He, T. F. Didar, Z. Hosseinidoust, *Smart Med.* **2022**, *1*, 20220015; b) Y. Gao, Q. Ma, *Smart Med.* **2022**, *1*, 20220012.

[11] a) Y. Chen, D. Qin, J. Zou, X. Li, X. D. Guo, Y. Tang, C. Liu, W. Chen, N. Kong, C. Y. Zhang, W. Tao, *Adv. Mater.* **2023**, *35*, 2207787; b) J. Ouyang, X. Ji, X. Zhang, C. Feng, Z. Tang, N. Kong, A. Xie, J. Wang, X. Sui, L. Deng, Y. Liu, J. S. Kim, Y. Cao, W. Tao, *Proc. Natl. Acad. Sci. U. S. A.* **2020**, *117*, 28667; c) N. Farokhzad, W. Tao, *Trends Chem.* **2021**, *3*, 589; d) J. Ouyang, A. Xie, J. Zhou, R. Liu, L. Wang, H. Liu, N. Kong, W. Tao, *Chem. Soc. Rev.* **2022**, *51*, 4996.

[12] N. Kim, E. Kim, H. Kim, M. R. Thomas, A. Najer, M. M. Stevens, *Adv. Mater.* **2021**, *33*, 2007738.

[13] I. Ocsoy, S. Yusufbeyoglu, V. Yilmaz, E. S. McLamore, N. Ildiz, A. Ulgen, *Colloids Surf., B* **2017**, *159*, 16.

[14] a) J. Wang, H. Wang, H. Wang, S. He, R. Li, Z. Deng, X. Liu, F. Wang, *ACS Nano* **2019**, *13*, 5852; b) J. Wang, S. Yu, Q. Wu, X. Gong, S. He, J. Shang, X. Liu, F. Wang, *Angew. Chem., Int. Ed.* **2021**, *60*, 10766.

[15] a) F. M. Husain, F. A. Qais, I. Ahmad, M. J. Hakeem, M. H. Baig, J. M. Khan, N. A. Al-Shabib, *Appl. Sci.* **2022**, *12*, 710; b) H. Wu, H. Tian, J. Li, L. Liu, Y. Wang, J. Qiu, S. Wang, S. Liu, *Composites, Part B* **2020**, *202*, 108415.

[16] E. T. Sarcan, M. Silindir-Gunay, A. Y. Ozer, *Int. J. Pharm.* **2018**, *551*, 329.

[17] P. Ostroverkhov, A. Semkina, V. Naumenko, E. Plotnikova, R. Yakubovskaya, S. Vodopyanov, A. Abakumov, A. Majouga, M. Grin, V. Chekhonin, M. Abakumov, *Pharmaceutics* **2018**, *10*, 284.

[18] L. Wang, C. Hu, L. Shao, *Int. J. Nanomedicine* **2017**, *12*, 1227.

[19] H. Dong, W. Xiu, L. Wan, Q. Li, Y. Zhang, M. Ding, J. Shan, K. Yang, Z. Teng, L. Yuwen, Y. Mou, *Chem. Eng. J.* **2023**, *453*, 139839.

[20] H. Zhao, Z. Zhang, D. Zuo, L. Li, F. Li, D. Yang, *Nano Lett.* **2021**, *21*, 5377.

[21] M. Ran, Z. Gounani, J. Yan, J. M. Rosenholm, H. Zhang, *Nano Sel.* **2022**, *3*, 1201.

[22] A. Heydorn, A. T. Nielsen, M. Hentzer, C. Sternberg, M. Givskov, B. K. Ersbøll, S. Molin, *Microbiology* **2000**, *146*, 2395.

[23] A. Sulaiman, S. McGarry, S. El-Sahli, L. Li, J. Chambers, A. Phan, M. Cote, G. O. Cron, T. Alain, Y. Le, S. H. Lee, S. Liu, D. Figeys, S. Gadde, L. Wang, *Mol. Cancer Ther.* **2019**, *18*, 1755.